RSC Advances

PAPER

View Article Online
View Journal | View Issue

Cite this: *RSC Adv.*, 2021, **11**, 36265

Preparation of aramid-based epoxy resin from low-grade aramid†

Changlei Yu,[b] Pengda Yu,[a] Gang Ma,[a] Lequn Zhou,[b] Fei Deng,[c] Fang Wang[c] and Xinbao Zhu *[ab]

Received 14th October 2021
Accepted 1st November 2021

DOI: 10.1039/d1ra07602g

rsc.li/rsc-advances

Low-grade aramid fibers, an unavoidable by-product in the industrialized process of aramid fiber production, are difficult to utilize and harmful to the environment. In this study, low-grade aramid fibers were recycled to assemble a high-quality epoxy resin through an epoxidation modification. Triggered by the epichlorohydrin, the molecular configuration of the low-grade aramid fibers was altered through crosslinking and chain-extension processes. bisphenol-A epoxy resin (E-51) with 5% aramid-based epoxy resin cured product exhibited improved mechanical and thermal properties, outperforming pure E-51 and pure aramid. This improvement is caused by the increased percentage of epoxide groups and flexible ether bonds. This work opens up new possibilities to maximize the reclamation of low-grade aramid fibers, which currently poses an obstacle in waste recycling.

Introduction

Aramid fiber is a kind of high-molecular organic fiber with excellent physical and chemical properties.[1] It has high modulus, low density, high temperature resistance, and chemical corrosion resistance. As one of the reinforcements of composite materials, aramid fiber takes the forms of filament, chopped fiber, fabric, and pulp.[2–5] It is widely used in aerospace, sports equipment, electronic appliances, automobiles, special equipment, and other fields.[6–9]

Aramid fiber-reinforced polymer often refers to the laminated structure prepared by stacking aramid fiber and resin matrixes. Aramid fiber-reinforced polymer has the advantages of epoxy resin and aramid fiber, such as excellent specific strength and specific stiffness, outstanding impact, and fatigue resistance.[10–13] However, aramid fiber is usually incompatible with epoxy resin at the interface and has low surface roughness[14,15] because the molecular structure of aramid usually has an unbranched main chain and lack of active groups, which can make its surface of aramid highly ordered. Therefore, it is necessary to modify aramid in preparing functional aramid fiber by physical methods such as coating,[16,17] plasma,[18,19] high-energy rays,[20,21] supercritical fluid method,[22] or by chemical methods including copolymerization,[23,24] surface etching,[25] or surface grafting.[26–29]

A certain amount of aramid fiber is labeled as low-grade in the process of polymerization when the molecular weights of the aramid polymers fail to meet the spinning requirements, which was influenced by various factors such as raw materials, equipment, or operation technologies. It is often discharged directly as solid wastes owing to its non-utility. Unlike other combustible wastes, low-grade aramids are physically hard to incinerate and are also prone to decay. The research on the recycling of low-grade aramid fiber has deepened in recent years.[30] For example, those low-grade aramids could be applied to nanocomposites, adsorption materials, and building materials.[31–33] However, there is the rare literature report focused on assembling aramid fiber-reinforced polymer from low-grade aramids.

In this study, we have verified a smart method considering the molecular structure characteristic of the low-grade aramid fiber to prepare resin-based composite materials with a sharp increase in interface performance. The initial characteristic of the low-grade aramid can enhance the adhesion of aramid fiber and resin matrixes. To the best of our knowledge, this is the first time for preparation of a low-viscosity liquid aramid-based epoxy resin by activating a low-grade aramid with a metallization reagent, liquefying it with ethoxylation, and causing a reaction with epichlorohydrin.[34] Finally, we discovered that the mechanical and thermal properties of E-51 can be largely improved by adding aramid-based epoxy resin in different proportions. It is expected to be applied to the industrialized preparation of aramid-based composite materials in the future.

Experimental

Materials

Aramid, Sinopec Yizheng Chemical Fiber Co., Ltd; DMSO, methylene chloride, acetone, arsenic acid, hydrochloric acid, imidazole, diethylenetriamine, sodium methoxide, phthalic

[a]College of Chemical Engineering, Nanjing Forestry University, Nanjing 210037, People's Republic of China. E-mail: zhuxinbao@njfu.com.cn

[b]Anhui Epoxy Resin and Additives Engineering Technology Research Center, Huangshan, 245000, People's Republic of China

[c]Sinopec Yizheng Chemical Fiber Co., Ltd, Yizheng, 211900, People's Republic of China

† Electronic supplementary information (ESI) available. See DOI: 10.1039/d1ra07602g

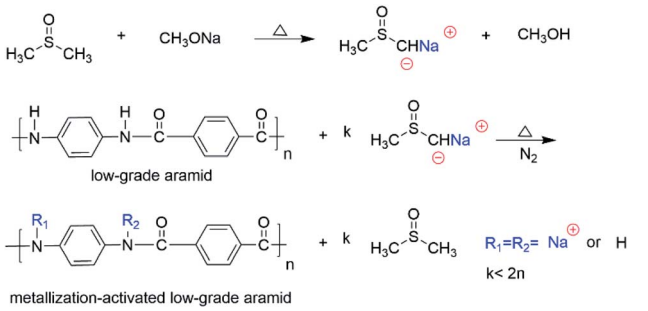

Scheme 1 Activation of low-grade aramid using metallization reagent.

anhydride, Nanjing Chemical Reagent Co., Ltd; ethylene oxide, Sinopec Yangzi Petrochemical Co. Ltd; epichlorohydrin, E51-epoxy resin, Anhui Hengyuan Chemical Co., Ltd.

Synthesis of aramid-based epoxy resin

We poured 300 mL of dimethyl sulfoxide into a 500 mL four-necked flask with a stirrer and reflux cooler. We then added 3.5 g of sodium methoxide and heated to 130 °C. Then 6 g of low-grade aramid powder was added under the protection of nitrogen. After 4 h of reaction, a dark brown solution was generated (Scheme 1). We used sodium methoxide instead of sodium hydride, which is convenient to use, causes less hydrogen production, and is safer.

An activated solution after a metallization reaction was added to the autoclave, and we performed N_2 replacement three times. Then the solution was stirred and heated to 110 °C. 20.6 g epoxyethane was slowly added and reacted for 2.5 h (Scheme 2). The low-grade aramid was liquefied, and the hydroxyl value of the ethoxylated modified aramid was 276.05 mg KOH/g.

The obtained ethoxylated aramid solution was put into a four-necked flask equipped with a stirrer, condenser, and thermometer. It was passed in N_2 and heated to 30 °C with stirring. We then dropped 11.90 g epichlorohydrin with a constant pressure funnel and heated to 50 °C for 4.5 h. The products were cooled to room temperature and extracted with dichloromethane. The extracts were distilled under reduced pressure to 120 °C to obtain a low-grade aramid-based epoxy resin with an epoxy value of 0.92 eq./100 g (Scheme 3).

Characterizations

Refer to standard "GB/T 1632-93 polymer dilute solution viscosity and intrinsic viscosity determination" to determine the viscosity of aramid.

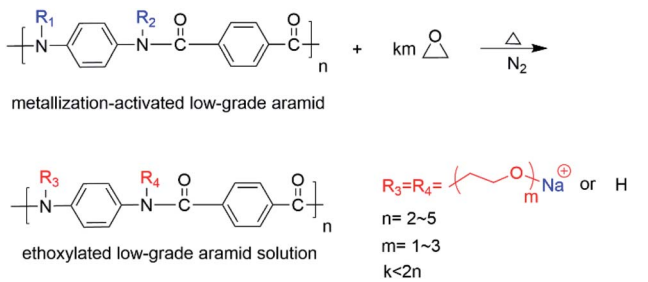

Scheme 2 Ethoxylation reaction of low-grade aramid.

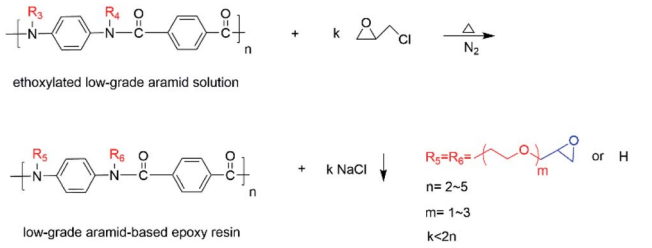

Scheme 3 Preparation of low-grade aramid-based epoxy resin.

Refer to standard "GB/T 12000.8-2009 determination of hydroxyl value of polyether polyols" to determine the hydroxyl value of polyols.

Refer to standard "GB/T 1677-2008 determination of plasticizer epoxy value" to determine the epoxy value of aramid-based epoxy resin.

Infrared Radiation (IR) of samples were determined by using Nicolet FT-IR360 Fourier Infrared Spectrometer from United States. The solid samples were compressed with KBr, and the scanning range was 400–4000 cm^{-1}.

Nuclear magnetic resonance (NMR) of samples were measured by Brucker AVANeE400 from Switzerland with $CDCl_3$ as the solvent.

Tensile strength was tested according to GB/T1040-92, using type II specimens. Impact strength and bending strength were tested according to GB/T1043-93, using unnotched specimens. The size was 4 mm × 10 mm × 80 mm.

The thermal stability of samples was displayed by Netzsch TG209C thermogravimetric analyzer from German. The temperature range was 30–800 °C, the heating rate was 10 °C min^{-1}, and the flow rate was 40 mL min^{-1} under nitrogen protection.

The glass transition temperature of samples was tested by PerkinElmer Differential Scanning Calorimeter (DSC) STA4490C from United States. Temperature range was 20–200 °C, and the heating rate was 20 °C min^{-1} under the protection of nitrogen atmosphere.

The fractured surface morphologies of samples were obtained by JEM-1400 transmission microscope from JEOL Ltd. Specimens were cut out to an appropriate size and the fractured surface was sprayed with gold.

Results and discussion

Low-grade aramid fiber characterization

Aramid fibers were divided into high-grade, middle-grade, and low-grade aramids based on their molecular weights. Low-grade aramids with a molecular weight near 2606 amu. were usually considered as waste in the industrial production process. This relationship is systematically presented with high grade and middle grade as reference.

Viscosity test. Aramids with different molecular weights also have different degrees of polymerization. We investigated the viscosities of high-grade, middle-grade, and low-grade aramids. As shown in Fig. 1, we plotted with *C* and extrapolated two lines

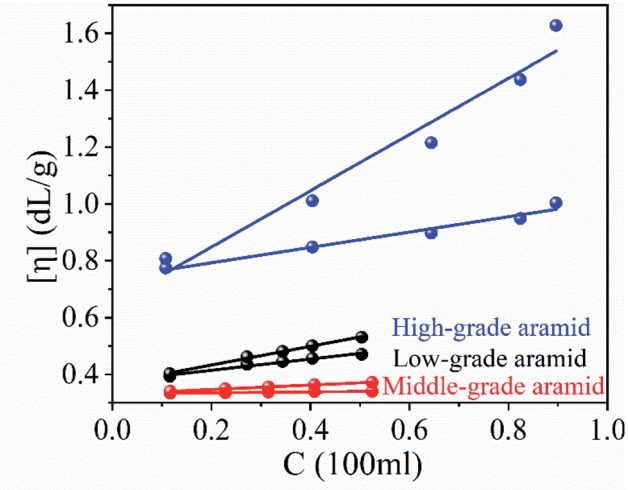

Fig. 1 Intrinsic viscosities of low-grade, middle-grade, and high-grade aramids (plot with η_{sp}/C *vs.* C and extrapolate to the intercept of $C \rightarrow 0$; to plot with ln η_r/C *vs.* C, extrapolate to the intercept, $C \rightarrow 0$, and the two lines meet at one point.).

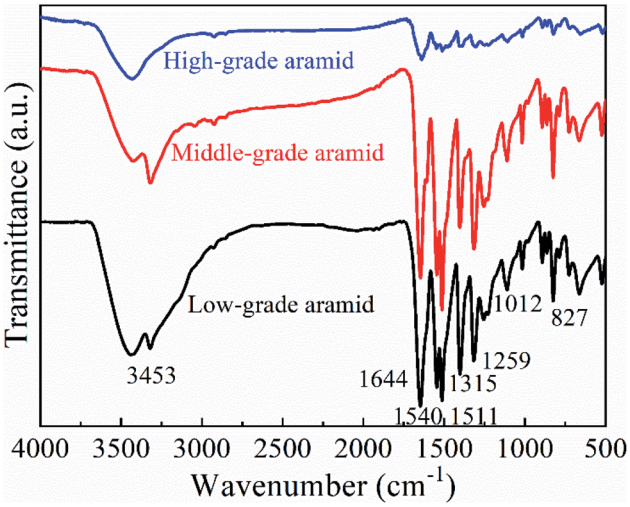

Fig. 2 Infrared spectra of low-grade, middle-grade, and high-grade aramids.

to converge at one point to obtain their intrinsic viscosities. The viscosity-average molecular weight and degree of polymerization were calculated according to the following formula:[35,36]

$$[\eta] = 7.9 \times 10 - 5M_{\eta}1.06 \quad (1)$$

$$\mathrm{DP}_{\eta} = \frac{M_{\eta}}{238} \quad (2)$$

The average linear correlation coefficients of low-grade, middle-grade, and high-grade aramids show a good linear relationship in Fig. 1. It can be seen from Table 1 that the viscosities of low-grade and middle-grade aramids were similar, and the corresponding viscosity-average molecular weight and degree of polymerization were also similar, whereas high-grade aramid showed twice-higher figures than that of the other two samples. As expected, low-grade aramids had a relatively worse viscosity property.

Infrared analysis. The infrared spectra of low-grade, middle-grade, and high-grade aramids appear in Fig. 2. We confirmed that the infrared spectra of low-grade, middle-grade, and high-grade aramids were similar except for the weaker pattern in the high-grade aramid. The secondary amide's free and associated N–H stretching vibration peaks were near 3400 cm^{-1}. The amide band's C=O stretching vibration peak was located near 1644 cm^{-1}. Absorption peaks at 1540 cm^{-1} and 1511 cm^{-1} were caused by the CN/NH stretching vibration, which was an amide II band. The absorption peak at 1315 cm^{-1} was caused by CN stretching vibration, which was from an amide III band. The absorption peaks at 1259 cm^{-1} and 1012 cm^{-1} were the in-plane and out-of-plane bending vibration peaks of a benzene ring, and the absorption peaks near 827 cm^{-1} were the characteristic peaks of a *para*-substituted benzene ring. The aforementioned structures were aromatic amide characteristic absorption peaks, indicating that the molecular structure of low-grade, middle-grade, and high-grade aramids were all *para*-aramid and their molecular structures were the same except for the difference in their degree of polymerization.[37]

Table 1 $[\eta]$, M_{η} and DP_{η} of low-grade, middle-grade, and high-grade aramids

Aramid	$[\eta]$ (dL g^{-1})	M_{η} (amu)	DP_{η}
Low-grade aramid	0.33	2606	11
Middle-grade aramid	0.37	2903	12
High-grade aramid	0.69	5226	22

Thermogravimetric analysis. TG analysis of low-grade, middle-grade, high-grade aramids is shown in Fig. 3. In the early stage, low-grade, middle-grade, and high-grade aramids all had a small amount of quality loss at about 100 °C. The loss

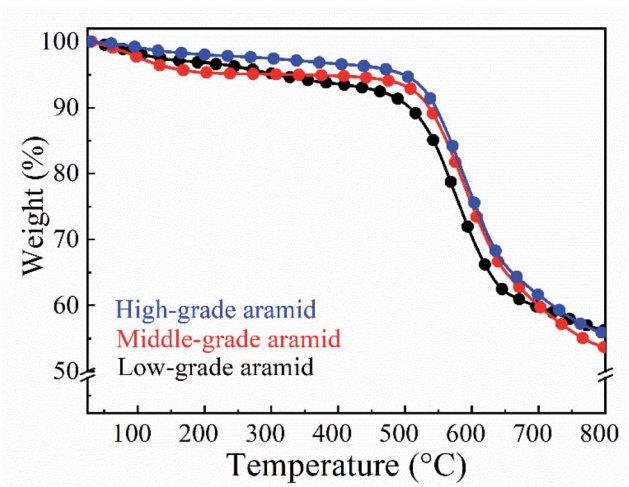

Fig. 3 Thermogravimetric curve of low-grade, middle-grade, and high-grade aramids.

of low-grade, middle-grade, and high-grade aramid was approximately 2%, 3%, and 1%, respectively, which was mainly caused by the evaporation of water adsorbed in the powder. Maximum weight loss rate temperature of the three was around 580 °C (DTG diagram is shown in Fig. S5†). The corresponding temperatures for low-grade, middle-grade, and high-grade aramids were 501 °C, 533 °C, and 543 °C, respectively, when the mass loss was 10%. The low-grade aramids with lower molecular weight were relatively inferior in heat resistance due to the difference in degree of polymerization and molecular weights.

Aramid-based epoxy resin characterization

We prepared an aramid-based epoxy resin through the metallization, ethoxylation, and epoxidation of low-grade aramid powders. We confirmed the ethoxylation and epoxidation products with infrared spectroscopy.

Infrared analysis. As shown in Fig. 4, double peaks at 3422 cm^{-1} and 3324 cm^{-1} were presented as the stretching vibration peaks of NH_2 on the low-grade aramid, whereas a larger absorption peak at 3353 cm^{-1} for the aramid-based epoxy resin was the OH stretching vibration peak. This illustrated that H on NH_2 was replaced with ethylene oxide. The absorption peak at 3072 cm^{-1} was the stretching vibration peak of a methylene group, and the presence of methylene on the aramid indicated that epoxyethane had been grafted onto the aramid. Moreover, the presence of amide marked the low-grade aramid with a strong C=O absorption peak at 1646 cm^{-1}, that is, the secondary amide I band, because the hydrogen on the amide bond was substituted and grafted by weakening the absorption peak of the polyol. The strong absorption peak at 1101 cm^{-1} was the secondary alcohol C–O stretching vibration absorption peak. In summary, the graphic shows that the reaction of low-grade aramid with sodium methoxide was successful, and epoxyethane was successfully anchored onto the amide bond.

As shown in Fig. 5, double peaks at 3422 cm^{-1} and 3324 cm^{-1} presented as stretching vibration peaks of NH_2 on the low-grade aramid, whereas a larger absorption peak at 3353 cm^{-1} for the aramid-based epoxy resin was an OH stretching vibration peak, indicating that H on NH_2 was replaced with epichlorohydrin. The strong absorption peak at 2861 cm^{-1} was the stretching vibration peak of the methylene group, indicating that epoxyethane had been grafted onto the aramid. Besides, the NH bending vibration peak was described at 1542 cm^{-1} and disappeared after the reaction, indicating that sodium methoxide was successfully modified and grafted to epoxyethane. Additionally, a sharp absorption peak appeared at 952 cm^{-1}, which was an epoxy absorption peak, indicating that the aramid-based polyether capping reaction had successfully attached epoxy groups. On the contrary, the sharp peak at 1114 cm^{-1} was the secondary alcohol's C–O stretching vibration, and the absorption peak at 1016 cm^{-1} was the C–O–C stretching vibration peak, indicating there were hydroxyl groups in the sample and the epoxy could not be completely terminated. The presence of amide caused the aramid to have a strong C=O absorption peak at 1644 cm^{-1} or the secondary amide I band. Because the hydrogen on the amide bond was substituted and grafted, this absorption peak was weakened.[37]

Nuclear magnetic analysis. As displayed in Fig. 6a, the triple peaks at 3.537 ppm and 3.535 ppm were the absorption peaks of methylene linked with amide, which indicated that ethylene oxide is grafted on the aramid fiber. The two small peaks at 6.462 and 6.466 ppm were the absorption peaks of H on aramid benzene ring. The chemical shifts of 3.246 ppm and 3.446 ppm should be the hydrogen on the amide not involved in the reaction. As displayed in Fig. 6b, there was a splitting peak at the chemical shift of 3.487 ppm representing the methylene group on the epoxy group, indicating that epichlorohydrin had blocked the hydroxyl group of the polyether and successfully introduced the ring on the surface of the aramid. The triple peaks at 3.550 ppm and 3.516 ppm were the absorption peaks of methylene linked with amide, which indicated the presence of methylene and ethylene grafted onto the aramid. The chemical

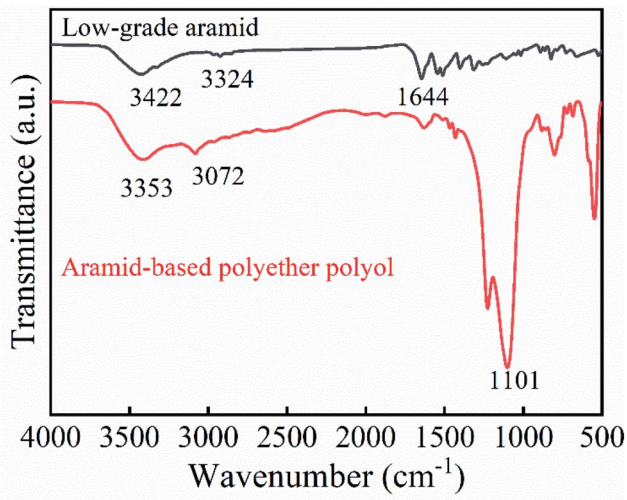

Fig. 4 Infrared spectra of aramid-based polyether polyol and low-grade aramid.

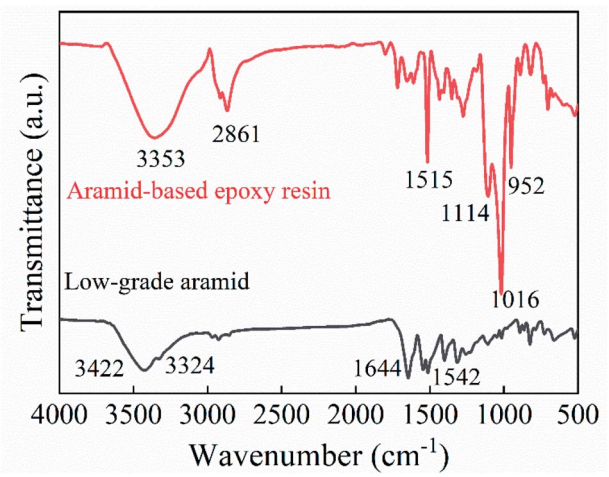

Fig. 5 Infrared spectra of the aramid-based epoxy resin and low-grade aramid.

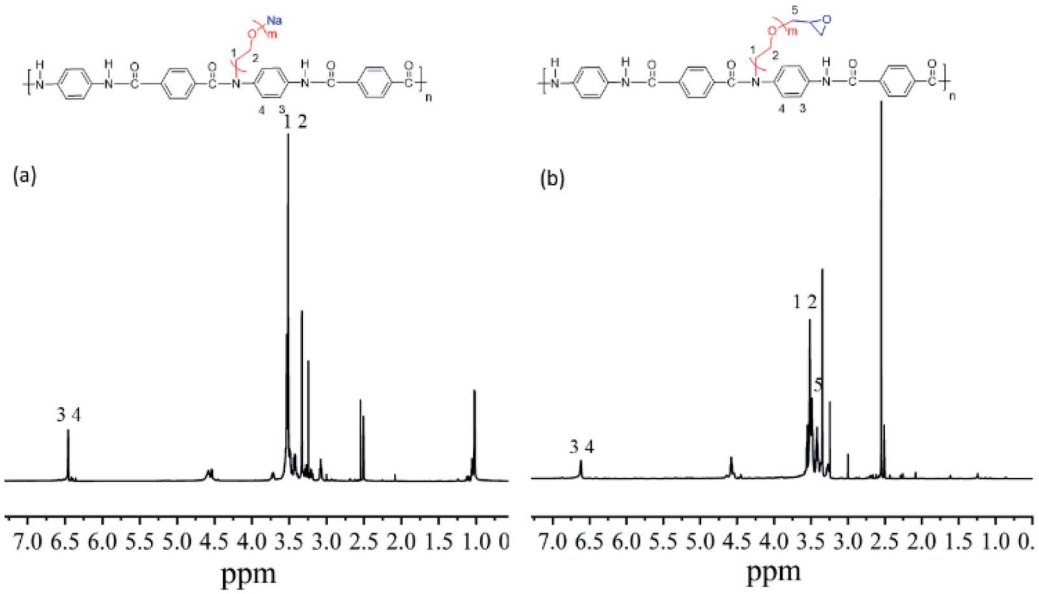

Fig. 6 The nuclear magnetic diagram of (a) aramid-based polyether polyol and (b) aramid-based epoxy resin.

shifts at 6.618 ppm and 6.616 ppm were H at position 3 and 4 on the benzene ring of the aramid.[38]

Effect of aramid-based epoxy resin on mechanical properties of cured products. We mixed the 2.5%, 5%, and 7.5% mass fractions of aramid-based epoxy resin with bisphenol-A epoxy resin (E-51) and cured the mixture with diethylenetriamine at 80 °C for 3 h. The mechanical properties of these cured products are illustrated in Fig. 7. The tensile strength, elongation at the break, and impact strength of the cured product indicate a trend of first increasing and then decreasing while increasing the amount of aramid-based epoxy resin added. When 5% aramid-based epoxy resin was added to E-51, the tensile strength, elongation at break, and impact strength were largely improved to 64.66 MPa, 3.45%, and 12.91 kJ m^{-2}, respectively, which were significantly increased by 65%, 88%, and 90%, respectively, compared with bare E-51. However, the bending strength and bending modulus showed an opposite trend. When 5% aramid-based epoxy resin was added to E-51, the bending strength and bending modulus were reduced by 12% and 11% respectively, compared with blank E-51. The introduction of rigid aramid structure to the crosslinked molecular chain made the hybrids harder to break when encountering an external force, which led to a significant increase of tensile strength. With the increase of aramid content, the powder compatibility became worse, and the crosslinking density decreased, resulting in the decline of mechanical properties. Compared to the pure E-51, alkyl chains on the surface of the aramid-based epoxy resin made the hybrids more likely to deform, resulting in the large increase of elongation at the break. Moreover, when subjected to external impact, the molecular chain with alkyl chain was prone to curl deformation, which could better absorb the external force and increase the impact strength.

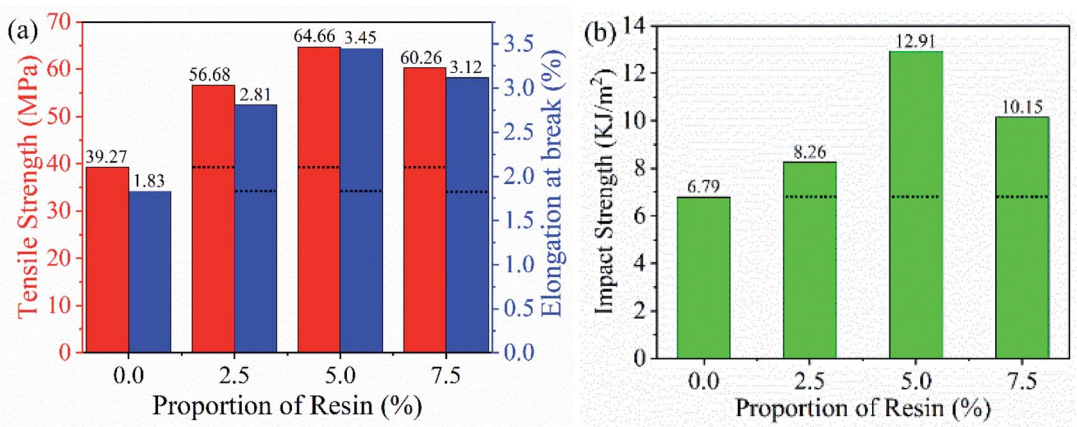

Fig. 7 The mechanical properties of cured products with E-51 and different proportions of aramid-based epoxy resin added (a) tensile strength and elongation at break (b) impact strength.

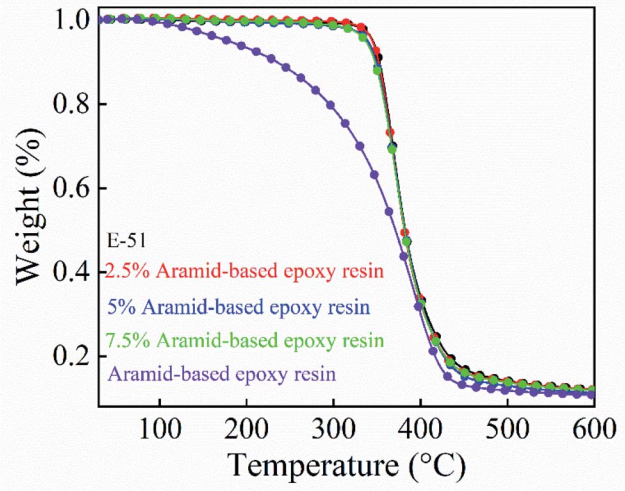

Fig. 8 The thermal weight loss curve of cured products with E-51 and different proportions of aramid-based epoxy resin added.

Thermal stability. A thermal weight loss test is usually used to measure the thermal stability of materials. In this study, the original E-51 and the cured products with E-51 and different proportions of aramid-based epoxy resin added were investigated. Thermal weight loss curves are shown in Fig. 8, and the thermal weight loss characteristic temperature is shown in Table 2. We set the decomposition temperature at 5% mass loss as the initial temperature and the decomposition temperature at 50% mass loss as a reference point to illustrate the thermal stability of the composite material. It can be seen from Fig. 8 and Table 2 that the decomposition temperatures at 5% and 50% mass loss (T5% and T50%) both showed a slightly downward trend when increasing the proportions of aramid-based epoxy resin added. Compared with T5% of pure E-51, the T5% of the 2.5%, 5%, and 7.5% aramid-based epoxy resin added cured products decreased by 0.7 °C, 5.78 °C, and 8.45 °C, respectively. Compared with the T50% of blank E-51, T50% of the 2.5%, 5%, and 7.5% aramid-based epoxy resin with added cured products decreased slightly by 0.81 °C, 0.92 °C, and 0.93 °C, respectively. With the increase of aramid-based epoxy resin, more alkyl groups on the side chain were introduced into the hybrids, which diminished the proportion of benzene rings. As is known, the thermal stability of a flexible alkyl chain is lower than that of a benzene ring,[39] which made the thermal stability of the hybrids slightly lower than pure E-51. In addition, the more aramid-based epoxy resin introduced in the blends, the more EO bonds involved. Even though the aramid content was also increased and thus it might cause the decrease of the char yield with a higher aramid-based epoxy resin content.

Table 2 Thermal weight loss characteristic temperature of cured products with E-51 and different proportions of aramid-based epoxy resin added

Name	T5% (°C)	T50% (°C)
Aramid-based epoxy resin	178.41	371.10
E-51	345.18	382.22
2.5% Aramid-based epoxy resin	344.48	381.41
5% Aramid-based epoxy resin	339.40	381.29
7.5% Aramid-based epoxy resin	336.73	381.28

Glass transition temperature. Glass transition temperature (T_g) is used to measure the thermomechanical properties of amorphous polymers. It reflects the change of temperature for the molecular chain from freezing to thawing and it often affects the scope of application for the polymer. In this study, we measured the T_g of pure E-51 and the cured products with E-51 and different proportions of aramid-based epoxy resin added by using differential scanning calorimetry (DSC). As shown in Fig. 9, as the proportion of aramid-based epoxy resin added increased, the glass transition temperature of the cured product would show first a downward and then an upward trend. When the proportion of aramid-based epoxy resin added in E-51 was 7.5%, the T_g of the composite material was higher than that of blank E-51. The addition of a flexible alkyl chain from an aramid-based epoxy resin helped with lubrication so that the flexible chain could thaw at a lower temperature, resulting in the decrease of the T_g of the hybrids at the beginning. With the gradual increase of aramid-based epoxy resin, the curling movement of the alkyl chain was restrained with the rising temperature, resulting in the increase of the thawing temperature. Therefore, the excessive aramid epoxy resin would cause the T_g of the hybrids to be higher than that of the E-51. As a control experiment, we found out that the pure aramid-based epoxy resin cannot be cured with diethylenetriamine and stay liquified.

Scanning electron microscope. The morphology of the fracture surface of the material could reflect the fracture type of the material, and the microstructure could be used to evaluate the type of fracture. In this study, the fracture surface of pure E-51 and the 5% aramid-based epoxy resin added cured product were selected for analysis. The fracture surface of the original E-51 in

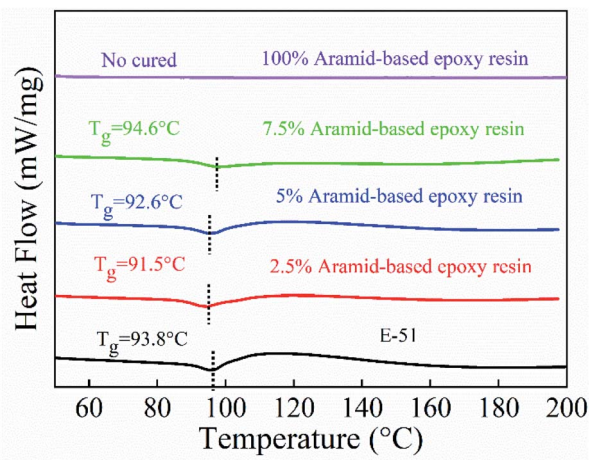

Fig. 9 The DSC curve of cured products with different addition proportions of aramid-based epoxy resin.

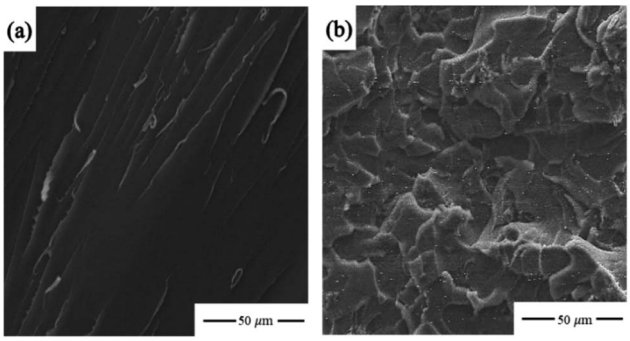

Fig. 10 Fracture surface SEM of (a) E-51 and (b) 5% aramid-based epoxy resin added.

Fig. 10a was relatively smooth and brittle because the blank E-51 resin after curing had a molecular chain structure of mostly benzene. When it was hit externally, the inflexible molecular chain structure of led to brittle fracture. On the fracture surface of the 5% aramid-based epoxy resin added cured product in Fig. 10b, there were more micro-cracks. When struck by an external force, the micro-cracks could diffuse into their surroundings to absorb energy, and the impact strength was improved owing to a ductile fracture. The addition of aramid-based epoxy resin in E-51 introduced an epoxide functional group and flexible ether bond, which largely increased the compatibility of with epoxy resin. In addition, aramid-based epoxy resin retained a skeleton structure of aramid, which maintained its compatibility with other aramids. It can be used as a bridge to better connect aramid and epoxy resin, thereby improving the overall performance of the composite materials.

Conclusions

In summary, we successfully transformed low-grade aramid fiber to high value-added aramid-based epoxy resin in a cost-effective and environmentally friendly way, which promoted the sustainable development of industrial aramid fiber production. We were the first group to prepare aramid-based epoxy resin by using low-grade aramid fiber as raw material and activating it with a sodium methoxide metallization reagent. Coupled with only 5% low-grade aramid, the hybrids exhibited unexpected enhancement in the tensile strength, elongation at break, and impact strength, with 64.66 MPa, 3.45%, and 12.91 kJ m^{-2} respectively, which were 65%, 88% and 90% higher respectively than those of pure E-51. Meanwhile, the thermal stability of this product remained unchanged with the increase of aramid-based epoxy resin in E-51. SEM revealed that the impact strength significantly improved owing to the introduction of more epoxide functional groups and flexible ether bonds from aramid-based epoxy resin, which allowed ductile fractures. Moreover, aramid-based epoxy resin maintained the skeleton structure of the aramid fiber, which had good compatibility with both epoxy resin and aramid fiber. In the future, aramid-based epoxy resin has the potential to be used as an adhesion agent to prepare aramid and epoxy resin related composites.

Conflicts of interest

There are no conflicts to declare.

Acknowledgements

The authors are grateful for funding received from Jiangsu Province Key R&D Program (BE2019111) and the National Key R&D Program of China (2018YFD0600402). Authors are also grateful to Priority Academic Program Development of Jiangsu Higher Education Institutions (PAPD) for their financial support.

Notes and references

1 H. Kong, R. Zhang, J. Zhou, Y. Ma, C. Teng and M. Yu, *Progress of Materials in China*, 2013, **11**, 676–684.
2 A. K. Dwivedi, M. W. Dalzell, S. A. Fossey, K. A. Slusarski, L. R. Long and E. D. Wetzel, *Int. J. Impact Eng.*, 2016, **96**, 23–34.
3 B. Wang, G. Ding, G. Wang and S. Kang, *J. Compos. Mater.*, 2020, **54**(25), 3883–3893.
4 X. Zhang, T. Li, Z. Wang, H. Peng and J. Lin, *Prog. Org. Coat.*, 2021, **151**, 106088.
5 Q. Xu, H. Kong, H. Ding, J. Zeng and M. Yu, *Polym. Compos.*, 2020, **42**(3), 1473–1485.
6 S. M. Khajamoinuddin, A. Chatterjee, M. R. Bhat, D. Harursampath and N. Gundiah, *J. Compos. Mater.*, 2021, 002199832110115.
7 X. Li, Q. Sun, S. Wang and H. Tang, *Text. Res. J.*, 2021, 004051752110106.
8 K. Kumar, S. N. Mandleywala, M. P. Gannon and N. Estes, *Clin. J. Sport Med.*, 2017, **27**(1), 26–30.
9 J. Lyu, M. D. Hammig, L. Liu, L. Xu, H. Chi, C. Uher and T. Li, *Appl. Phys. Lett.*, 2017, **111**(16), 161901.
10 X. Tang, H. Tan and Y. Wang, *Eng. Plast. Appl.*, 2013, **2**, 8–12.
11 S. D. Salman, Z. Leman, M. Sultan and M. Ishak, *Text. Res. J.*, 2016, **87**(17), 2051–2065.
12 S. Bazhenov, *J. Mater. Sci.*, 1997, **32**(15), 4167–4173.
13 Z. Wang and X. Fu, *Science and technology information*, 2011, **21**, 58.
14 S. Rebouillat, J. B. Donnet and K. W. Tong, *Polymer*, 1997, **38**(9), 2245–2249.
15 P. E. Cassidy, *Thermally Stable Polymers Synthesis & Properties*, 1980.
16 Q. Ni, Y. Fu, J. Chen, X. Zhu and F. Yao, *Appl. Surf. Sci.*, 2014, **321**(321), 103–108.
17 J. Zhu, L. Yuan, Q. Guan, G. liang and A. Gu, *Chem. Eng. J.*, 2017, **310**, 134–147.
18 Y. Sun, Q. Liang, H. Chi, Y. Zhang, S. Yi, D. Fang and F. Li, *Fibers Polym.*, 2014, **15**(1), 1–7.
19 W. Fan, H. Tian, H. Wang, T. Zhang, X. Yang, Y. Yu, X. Meng, X. Yu and B. Xu, *Polym. Test.*, 2018, **72**, 147–156.

20 F. Xie, L. Xing, L. Liu, Z. Zhong, C. Jia, W. Wang, W. Wang and Y. Huang, *J. Appl. Polym. Sci.*, 2017, **134**(23), 1–9.
21 A. Jn, A. Lag, B. Lz and C. Hsab, *Carbon*, 2020, **158**, 146–156.
22 L. Zhang, H. Kong, M. Qiao, X. Ding and M. Yu, *Appl. Surf. Sci.*, 2020, **521**, 146430.
23 W. Wang, X. Qi, Y. Guan, F. Zhang, J. Zhang, C. Yan, Y. Zhu and X. Wan, *J. Polym. Sci., Part A: Polym. Chem.*, 2016, **4**(13), 2050–2059.
24 K. Luo, Y. Wang, J. Yu, J. Zhu and Z. Hu, *Mater. Sci. Forum*, 2017, **898**, 2174–2180.
25 G. Lin, H. Wang, B. Yu and G. Qu, *Mater. Chem. Phys.*, 2020, **255**, 123486.
26 F. Pan, R. Qu, X. Jia, H. Sun, K. An, Y. Mu, C. Ji and P. Yin, *Appl. Surf. Sci.*, 2017, **416**, 225–233.
27 J. Luo, M. Zhang, B. Yang, G. Liu and J. Tan, *Carbohydr. Polym.*, 2019, **203**, 110–118.
28 T. Li, Z. Wang, H. Zhang and Z. Hu, *J. Compos. Mater.*, 2021, **55**(13), 1823–1834.
29 T. Liu, Y. Zheng and J. Hu, *J. Appl. Polym. Sci.*, 2010, **118**(5), 2541–2552.
30 I. Okajima, H. Okamoto and T. Sako, *Polym. Degrad. Stab.*, 2019, **162**, 22–28.
31 B. Yang, W. Li, M. Zhang, L. Wang and X. Ding, *ACS Nano*, 2021, **15**, 7195–7207.
32 Y. Wu, D. Ju, F. Wang and Y. Huang, *Polym. Adv. Technol.*, 2021, **32**(6), 2476–2486.
33 X. Xu and Y. Zheng, *CN. Pat.* CN107974235a, 2017.
34 X. Zhu, M. Yu, Y. Zhu and B. Xie, *EP. Pat.* 18889839.9, 2020.
35 X. Zhang, Master thesis, Nanjing Forestry University, 2015.
36 A. Tang, T. Zhou and Z. Sun, *Papermaking Sci. Technol.*, 2009, **28**(5), 33–36.
37 H. Kong, S. Ye, J. Liu, M. Qin, S. Li and W. Shen, *High tech fiber and application*, 2014, **39**(3), 15–20.
38 R. M. Silverstein, F. X. Webster, D. J. Kiemle and D. L. Bry Ce, *Spectrometric Identification of Organic Compounds*, 8th edn, Wiley, 1980.
39 N. Bothe, F. DöScher and J. Klein, *Polymer*, 1979, **20**(7), 850–854.